Biosensors and Bioelectronics 135 (2019) 95–101

Contents lists available at ScienceDirect

Biosensors and Bioelectronics

journal homepage: www.elsevier.com/locate/bios

Highly stable Ru-complex-grafted 2D metal-organic layer with superior electrochemiluminescent efficiency as a sensing platform for simple and ultrasensitive detection of mucin 1

Gui-Bing Hu, Cheng-Yi Xiong, Wen-Bin Liang, Yang Yang, Li-Ying Yao, Wei Huang, Wen Luo, Ruo Yuan*, Dong-Rong Xiao*

Key Laboratory of Luminescent and Real-Time Analytical Chemistry (Southwest University), Ministry of Education, College of Chemistry and Chemical Engineering, Southwest University, Chongqing 400715, PR China

ARTICLE INFO

Keywords:
2D metal-organic layers
MUC1
ECL immunosensor
$Ru(bpy)_3^{2+}$ derivatives

ABSTRACT

This work utilized ultrathin metal-organic layer (MOL) to immobilize luminophores for effectively shortening the ion/electron-transport distance and relieving the diffusional constraints of ion/electron, which greatly enhanced the ECL efficiency and intensity. Moreover, the MOL's immobilization amount of luminophores should be higher than these of bulk MOFs because MOLs possess more accessible postmodification sites for the luminophores with minimal diffusion barriers. As expected, our proof-of-concept experiment indicated that the Hf-MOL's loading number of $Ru(bpy)_2(mcpbpy)^{2+}$ was about 1.74 times that of a 3D mesoporous MOF (PCN-777), and the ECL efficiency and intensity of PEI@Ru-Hf-MOL were around 1.27 times and 14.5 times those of PEI@Ru-PCN-777, respectively. In view of these merits, this work utilized the prepared PEI@Ru-Hf-MOL as a highly efficient sensing platform for simple, rapid and sensitive detection of mucin 1, which exhibited a broad linearity from 1 fg/mL to 10 ng/mL and a low detection limit of 0.48 fg/mL. This work provided a practicable strategy to develop high-performance ECL materials, and therefore opened up a new avenue to design ultrasensitive ECL biosensors, which expanded the application potential of MOLs in ECL assays.

1. Introduction

Mucin 1 (MUC1) is an important glycosylated protein, and the abnormal expression of MUC1 is used as tumor markers in the clinical diagnosis of colorectal, pancreatic, and prostate cancer (Kufe, 2009). Thus, it is very meaningful to find an effective way to sensitively detect MUC1 for clinical tumor diagnosis (Bossche et al., 2010; Nath and Mukherjee, 2014). In comparison with several other techniques, for example, fluorescence (Cheng et al., 2009; Si et al., 2018), electrochemical (Wen et al., 2015; Wang et al., 2017a) and surface plasmon resonance spectroscopy (SPR) (Ferreira et al., 2008), the electrochemiluminescence (ECL) technology (Wu et al., 2014; Zhao et al., 2015b; Cao et al., 2015; Liu et al., 2015; Wang et al., 2018) has captured a growing attention owing to its simplicity, high detection sensitivity and low cost (Chen et al., 2017b; Li et al., 2017a).

As the most classic reagents of ECL, tris(2,2′-bipyridyl)ruthenium(II) ($Ru(bpy)_3^{2+}$) and its derivatives possess high ECL activity, superior stability (Sun et al., 2007). In order to obtain a strong ECL signal, abundant of nanomaterials (Kim and Kim, 2014; Liu et al., 2014; Lin et al., 2015; Li et al., 2018; Wang et al., 2016b; Yang et al., 2017) have been used to immobilize the $Ru(bpy)_3^{2+}$ derivatives. Compared with conventional nanomaterials as carriers, the well-ordered porosity and high surface area of metal-organic frameworks (MOFs) provided the intrinsic advantage in increasing the immobilization number of luminophores. Recently, Chi's group has synthesized a novel tris(bipyridine) ruthenium(II)-functionalized MOF to sensitively detect Hg^{2+} (Lin et al., 2015), and our group has used ZIF-8 (ZIF = zeolitic imidazolate framework) as carrier to immobilize self-enhanced ruthenium polyethylenimine (Ru-PEI) complex for ultrasensitive detection of telomerase activity (Xiong et al., 2017). However, these reported MOF-based ECL sensors also face some challenges. On the one hand, the leakage of luminophores during testing may reduce the stability of the ECL immunosensor based on MOF because the stability of most MOFs in water is low. On the other hand, the utilization ratio of $Ru(bpy)_3^{2+}$ derivatives and the immobilization amount of $Ru(bpy)_3^{2+}$ derivatives were limited due to the small pore size of most MOFs. More recently, to overcome these drawbacks, we have reported a feasible strategy to construct highly stable and sensitive ECL sensors by using ultrastable

* Corresponding authors.
E-mail addresses: yuanruo@swu.edu.cn (R. Yuan), xiaodr98@swu.edu.cn (D.-R. Xiao).

https://doi.org/10.1016/j.bios.2019.03.026
Received 15 January 2019; Received in revised form 13 March 2019; Accepted 14 March 2019
Available online 15 March 2019
0956-5663/

three-dimensional (3D) mesoporous luminescent functional MOF (Ru-PCN-777) (Fig. S1, PCN = porous coordination network) in our previous work (Hu et al., 2018). However, the long path of ion/electron migration and diffusional constraints of ion/electron within the 3D bulk MOFs (Song et al., 2010) inhibited the electrochemical activation of the interior luminophores. As a result, the utilization ratio of ECL luminophores was still limited in the 3D luminescence-functionalized MOFs. Therefore, it is imperative to seek new materials as carriers to immobilize luminophores for further increasing the utilization ratio of ECL luminophores and enhancing the immobilization amount of luminophores.

Metal-organic layers (MOLs) (Lan et al., 2017, 2018; Shi et al., 2017; Cao et al., 2017; Ding et al., 2017), also known as MOF nanosheets or coordination nanosheets (Lu et al., 2016; Zhao et al., 2018; Huang et al., 2017; Kong et al., 2018), are a two-dimensional (2D) version of MOFs (Easun et al., 2017; Furukawa et al., 2013) with thickness reduced to a few nanometers (Dong et al., 2015), which could relieve the diffusional constraints of ion/electron (Cao et al., 2016). Furthermore, compared with 3D bulk MOFs (Xiao et al., 2012; He et al., 2012; Li et al., 2017b), the ultrathin 2D MOLs could shorten the transportation length of ion/electron (Wang et al., 2017c), which makes the utilization ratio of luminophores greatly increasing. In addition, because MOLs exhibit more readily accessible postmodification sites for the luminophores with a small diffusion barrier, the MOL's loading amount of luminophores should be higher than that of 3D bulk MOFs. Thus, MOLs are an ideal platform to immobilize luminophores for enhancing the ECL efficiency and intensity. Because of the above advantages, we chose the Hf-MOL as carrier to immobilize Ru(bpy)$_2$(mcpbpy)$^{2+}$ (bpy = 2,2′-bipyridine, mcpbpy = 4-(4′-methyl-[2,2′-bipyridin]-4-yl)butanoic acid) on the Hf_6 cluster of Hf-MOL by solvent-assisted ligand incorporation (SALI) method (Cao et al., 2016; Deria et al., 2014, 2015; Chen et al., 2016) (Scheme 1) and successfully synthesized a novel and stable Ru-complex-grafted 2D MOL (Ru-Hf-MOL). In order to further increase the ECL intensity, polyethylenimine (PEI) was decorated onto Ru-Hf-MOL as coreactant (Wang et al., 2014; Gui et al., 2014). As expected, it was found that the Hf-MOL's immobilization number of Ru(bpy)$_2$(mcpbpy)$^{2+}$ was about 1.74 times that of PCN-777, the average ECL intensity of PEI@Ru-Hf-MOL was around 14.5 times that of PEI@Ru-PCN-777, and the ECL efficiency of PEI@Ru-Hf-MOL was calculated to be 7.6%, which increased by 27% compared with that of PEI@Ru-PCN-777 (6.0%).

Considering the above-mentioned superior properties of PEI@Ru-Hf-MOL, it was used as an ideal sensing platform for MUC1 detection. The target-induced proximity hybridization (Hu et al., 2012; Zhang et al., 2007; Li et al., 2012) was utilized as the quantitative way for MUC1 detection because this strategy is simple, rapid and no complicated procedures are required. Thus, this work utilized PEI@Ru-Hf-MOL to construct a highly stable ECL sensor with superior ECL efficiency based on target-induced proximity hybridization for simple, rapid, and ultrasensitive determination of MUC1. The principle of this method was displayed in Scheme 2. First, PEI@Ru-Hf-MOL was decorated onto the glass carbon electrode (GCE) surface by means of nafion. Then, the ferrocene (Fc) and Ab1 labeled single-stranded DNA (Fc-DNA1-Ab1, Ab1 = antibody) acting as a quencher was strongly absorbed on PEI@Ru-Hf-MOL by π-π stacking interactions between the Fc-DNA1-Ab1 and PEI@Ru-Hf-MOL (Zhang et al., 2014; Zhao et al., 2016, 2015c; Wang et al., 2017b; Parvin et al., 2017), which made the ECL emission of Ru(bpy)$_2$(mcpbpy)$^{2+}$ could be effectively quenched by Fc (the signal off state) and resulted in a low background signal. Finally, upon the introduction of MUC1 and Ab2 labeled single-stranded DNA (Ab2-DNA2) into the system, a proximate complex was rapidly formed by the target-induced proximity hybridization. Because PEI@Ru-Hf-MOL can hardly interact with the formed proximate complex, the proximate complex would detach from the PEI@Ru-Hf-MOL surface (Zhang et al., 2014; Zhao et al., 2016, 2015c; Wang et al., 2017b; Parvin et al., 2017), leading to the signal on state. As a result, the proposed sensor realized the simple, rapid and ultrasensitive determination of MUC1. This work using highly stable Ru-complex-grafted 2D MOL to increase ECL efficiency and intensity not only provides a new approach for developing high-performance ECL materials, but also demonstrates that the stable MOLs can serve as a promising platform to immobilize luminophore for constructing highly stable and sensitive ECL sensors, which may expand the applications of MOLs in bioanalysis.

2. Experimental section

2.1. Construction process of immunosensor

Before fabrication, the GCE was polished and cleaned as the previous literatures (Wang et al., 2015; Zhang et al., 2015). Next, the prepared PEI@Ru-Hf-MOL was coated on the electrode surface by means of nafion. After drying, 10 μL of the Fc-DNA1-Ab1 solution was incubated on the prepared electrode overnight at 4 °C. Then, 16 μL of hexanethiol (HT, 1 mM) was added into the prepared electrode 40 min at 37 °C for blocking the remaining active sites. The every resultant electrode was washed with PBS (pH 7.4) to remove the excess reagents.

2.2. Measurement procedure

To detect MUC1, 10 μL of MUC1 solution with concentrations linearly increasing and 10 μL of the Ab2-DNA2 solution were doped onto the prepared electrode, respectively. Then, the prepared electrode was incubated 50 min at 37 °C. Subsequently, the ECL signals were measured in an ECL detector cell with PBS (3 mL) at room temperature.

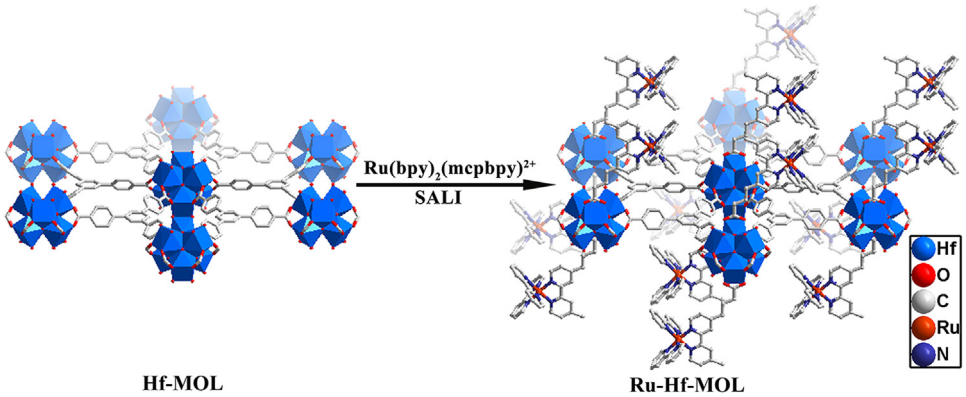

Scheme 1. Schematic representation of the grafting of Ru(bpy)$_2$(mcpbpy)$^{2+}$ onto Hf-MOL by the SALI method.

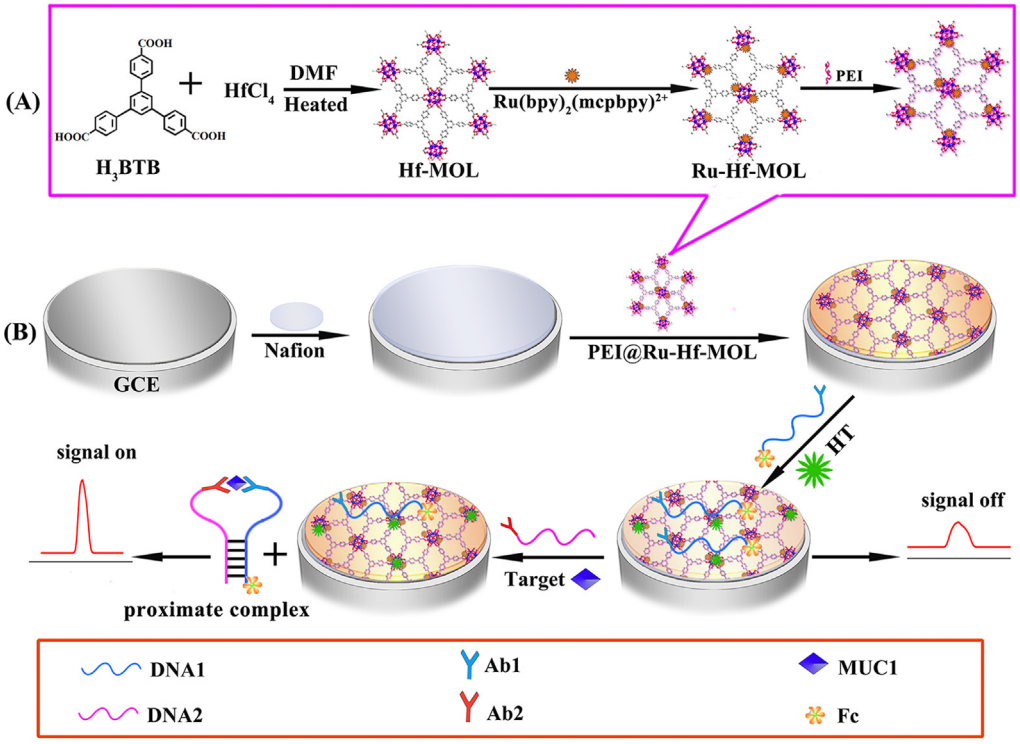

Scheme 2. (A) The synthesis of PEI@Ru-Hf-MOL and (B) the construction of the sensor.

3. Results and discussions

3.1. Characteristics of Hf-MOL and Ru-Hf-MOL

The prepared Hf-MOL and Ru-Hf-MOL were characterized by powder X-ray diffraction (PXRD), the scanning electron microscopy (SEM), transmission electron microscopy (TEM), atomic force microscopy (AFM), FTIR spectroscopy, and inductively coupled plasma-optical emission spectroscopy (ICP-OES). The PXRD patterns of Hf-MOL and Ru-Hf-MOL are consistent with the simulated PXRD pattern of Hf-MOL (Fig. S2). The SEM images of Hf-MOL and Ru-Hf-MOL indicate that the MOL is wrinkled ultrathin films (Fig. 1A and B). The TEM image of Ru-Hf-MOL (Fig. 1C) shows it ultrathin nature. The thickness of Ru-Hf-MOL was measured to be 1.4 ± 0.2 nm (Fig. 1D) by using AFM. The thickness of Ru-Hf-MOL was also found to be 4.2 ± 0.2 nm (Fig. S3), which corresponded to trilayer structures. Moreover, in comparison to $Ru(bpy)_2(mcpbpy)^{2+}$, the IR spectrum of Ru-Hf-MOL lacked the absorption peak at about 1710 cm^{-1} assigned to the protonated carboxylate groups (Fig. S4), demonstrating the carboxyl groups of $Ru(bpy)_2(mcpbpy)^{2+}$ were coordinated with the Hf^{4+}. It was found that 3.01 equiv of $Ru(bpy)_2(mcpbpy)^{2+}$ were incorporated per Hf_6 node within Hf-MOL and 1.73 equiv of $Ru(bpy)_2(mcpbpy)^{2+}$ were incorporated per Zr_6 node within PCN-777, which were measured by ICP-OES, and suggesting that the Hf-MOL's immobilization number of $Ru(bpy)_2(mcpbpy)^{2+}$ were around 1.74 times that of PCN-777. Through comparison, it was clearly found that the ultrathin 2D MOLs with minimal diffusion barriers provided an obvious advantage in increasing the loading capacity of luminophores.

3.2. The ECL intensities of PEI@Ru-Hf-MOL and PEI@Ru-PCN-777

The ECL intensities of PEI@Ru-Hf-MOL and PEI@Ru-PCN-777 were measured in the same experimental condition. As shown in Fig. S5B and Fig. S5C, the average ECL signals of PEI@Ru-PCN-777 and PEI@Ru-Hf-MOL were calculated to be 1109 au and 16120 au, respectively. This result indicated that the ECL intensity of PEI@Ru-Hf-MOL was around 14.5 times that of PEI@Ru-PCN-777, suggesting that the use of stable MOLs to load Ru(II) complex is an ideal approach for the construction of ECL materials with excellent performance.

3.3. The ECL efficiency of PEI@Ru-Hf-MOL and PEI@Ru-PCN-777

The ECL efficiency is defined as the number of photons transmitted per electron. And the ECL efficiency was calculated through the following relation (Wang et al., 2016a):

$$\Phi_x = \Phi_{st}\left(\frac{\int_0^t Idt}{\int_0^t idt}\right)_x \Big/ \left(\frac{\int_0^t Idt}{\int_0^t idt}\right)_{st} \quad (1)$$

Φ_x represents the ECL efficiency of sample, Φ_{st} stands for the ECL efficiency of $[Ru(bpy)_3]^{2+}$ (1 mM and 0.1 M (TBA)BF_4/acetonitrile) via annihilation, which is considered to be 5.0% (*I* stands for ECL intensity, *i* refer to current value). The ECL efficiencies of different ECL systems were calculated based on Eq. (1) and showed in Table 1. Obviously, the ECL efficiency of PEI@Ru-Hf-MOL is relatively high, which indicates that Ru-complex-grafted 2D MOLs could notably enhance the ECL efficiency by shortening the ion/electron-transport distance and decreasing the inner filter effect.

3.4. The possible ECL mechanism of the proposed ECL immunosensor

According to previous reported works (Zhuo et al., 2014; Zhao et al., 2015a), we proposed the possible mechanism of ECL process as follows (1)-(4):

$$[Ru^{2+}\text{-Hf-MOL}] - e^- \rightarrow [Ru^{3+}\text{-Hf-MOL}] \quad (1a)$$

$$PEI - e^- \rightarrow PEI^{\bullet +} \quad (1b)$$

$$PEI^{\bullet +} \rightarrow PEI^{\bullet} + H^+ \quad (2)$$

$$[Ru^{3+}\text{-Hf-MOL}] + PEI^{\bullet} \rightarrow [Ru^{2+*}\text{-Hf-MOL}] + PEI \quad (3)$$

$$[Ru^{2+*}\text{-Hf-MOL}] \rightarrow [Ru^{2+}\text{-Hf-MOL}] + h\nu \quad (4)$$

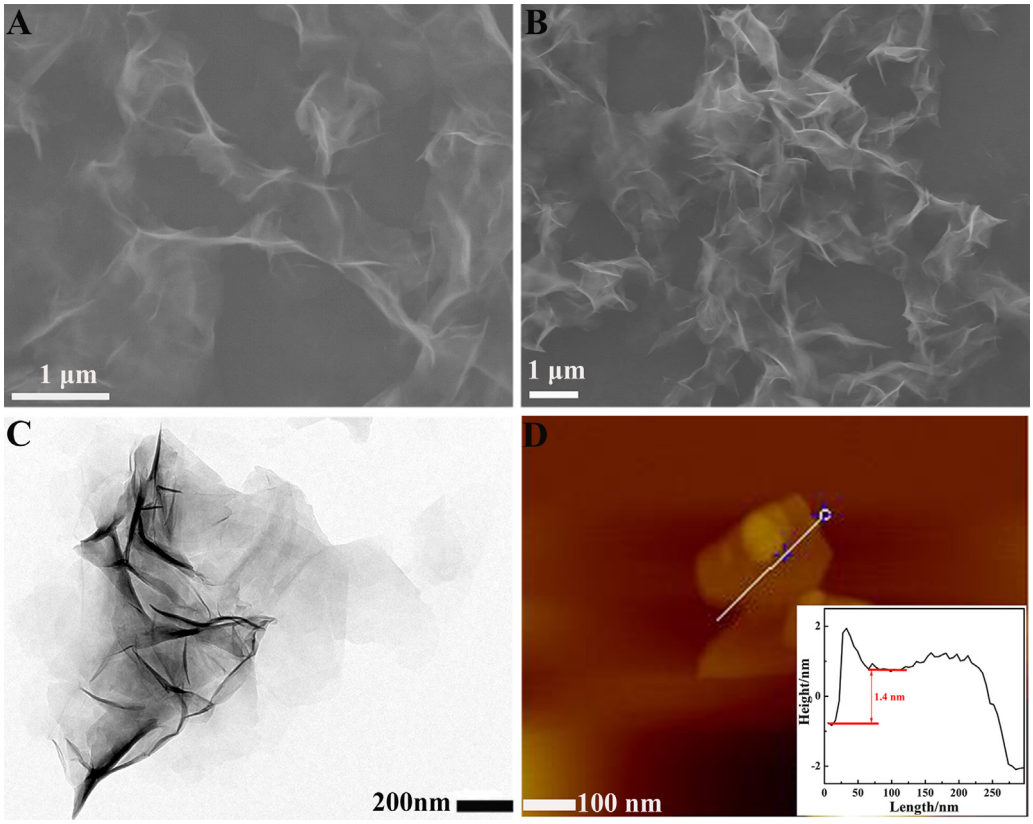

Fig. 1. The SEM images of Hf-MOL (A) and Ru-Hf-MOL (B); TEM image of Ru-Hf-MOL (C) and AFM image of Ru-Hf-MOL (D).

Table 1
ECL efficiencies of different ECL systems.

material	ECL efficiency	ref
○@CdInS	2.1%	Wang et al. (2016a)
Mn@CdInS	0.8%	
$Ru(bpy)_3Cl_2$/1 mM (annihilation)	5.0%	Chen et al. (2017a)
$Ru(mcbpy)(bpy)_2Cl_2$/particles	1.2%	
Ru-HPNSs	7.2%	
PEI@Ru-PCN-777	6.0%	this work
PEI@Ru-Hf-MOL	7.6%	

Ru-HPNSs = hollow porous polymeric nanospheres of a self-enhanced ruthenium complex.

3.5. Optimization of the reaction time

To obtain the best ECL immunosensor performance, we using 1 ng/mL MUC1 as an example to optimize the reaction time of Fc-DNA1-Ab1, MUC1 and Ab2-DNA2. From Fig. S6, the ECL intensity fulfilled a relatively stable value at 50 min. Thus, 50 min was chosen as the optimal reaction time in this experiment.

3.6. Characterization of the ECL immunosensor

To characterize the process of sensor modification, the ECL signal of each fabricated procedure were recorded. As exhibited in Fig. 2A, there was almost no ECL response for the GCE (curve a). Then, the ECL signal was greatly improved after the PEI@Ru-Hf-MOL was coated onto the electrode because of the superior property of PEI@Ru-Hf-MOL and the amplified effect of PEI as coreactant (curve b). However, the ECL intensity was almost the same as the GCE (curve c) after adding the Fc-DNA1-Ab1, which indicated that 2D MOL can strongly adsorb Fc-DNA1-Ab1 through π-π interactions, causing the effective quenching to the ECL emission and a low background intensity. Then, after the addition of HT, a further decreased ECL intensity was observed because of the insulation of HT (curve d). Finally, the ECL signal was increased again (curve e) when the electrode was incubated with MUC1 (1 pg/mL) and Ab2-DNA2 for the reason that the proximate complex detached from PEI@Ru-Hf-MOL.

Furthermore, cyclic voltammograms (CVs) were also used to confirm the modification process of the proposed immunosensor. As displayed in Fig. 2B, when nafion was modified on the electrode, the current greatly decreased (curve b) in comparison to the bare GCE (curve a) for the reason that nafion impeded the transfer of electrons. After the PEI@Ru-Hf-MOL was added onto the modified electrode, an increased redox peak current (curve c) was obtained because the large specific area of PEI@Ru-Hf-MOL could promote electron transfer. However, when the Fc-DNA1-Ab1 and HT was modified on the prepared electrode, redox peak currents were declined successively (curve d and e) because these biomacromolecules hindered the electron transfer. The results of ECL and CVs demonstrated that the proposed ECL sensor was modified as expected.

3.7. Analysis of MUC1

The prepared ECL sensor was used to detect MUC1 with different concentration. From Fig. 3A, the ECL signal increased with increasing MUC1 concentration from 1 fg/mL to 10 ng/mL. From Fig. 3B, the ECL intensity was proportional to the logarithm of the concentration of MUC1. The linear equation was $I = 9996.1 + 1498.3\lg c_{MUC1}$ with the correlation coefficient of 0.9992, and the detection limit was 0.48 fg/mL (signal/noise = 3), which was more sensitive than or comparable with the previously reported detection methods with signal amplification (Table 2). However, the prepared ECL sensor without signal amplification exhibits some obvious advantages over the previously reported sensors, such as simplicity, easier operation, shorter detection time, and broader linear range for MUC1 detection (Table 2). In

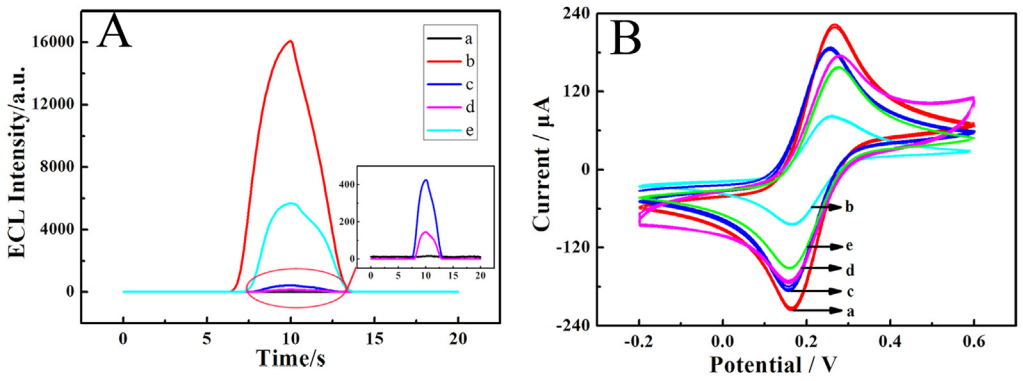

Fig. 2. (A) The ECL responses of different modified GCE: (a) bare GCE, (b) PEI@Ru-Hf-MOL/Nafion/GCE, (c) Fc-DNA1-Ab1/PEI@Ru-Hf-MOL/Nafion/GCE, (d) HT/Fc-DNA1-Ab1/PEI@Ru-Hf-MOL/Nafion/GCE, and (e) S2-Ab2-MUC1/HT/Fc-DNA1-Ab1/PEI@Ru-Hf-MOL/Nafion/GCE. (B) CVs curves in the presence of 5 mM $[Fe(CN)_6]^{3-/4-}$ of (a) bare GCE, (b) Nafion/GCE, (c) PEI@Ru-Hf-MOL/Nafion/GCE, (d) Fc-DNA1-Ab1/PEI@Ru-Hf-MOL/Nafion/GCE, (e) HT/Fc-DNA1-Ab1/PEI@Ru-Hf-MOL/Nafion/GCE.

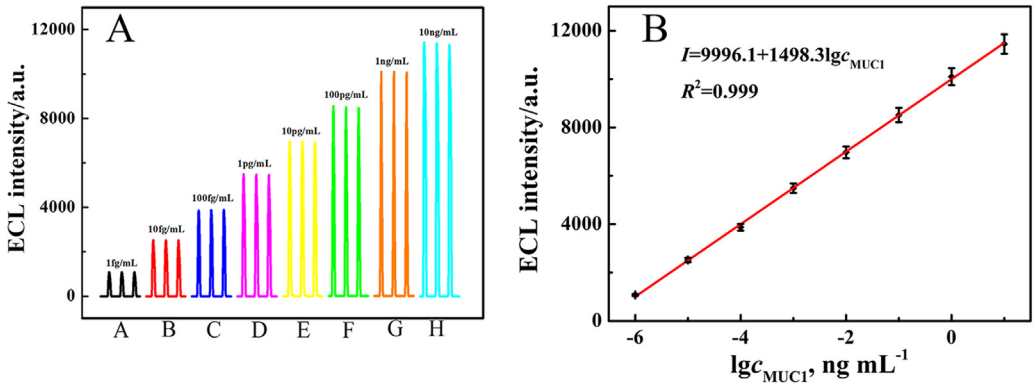

Fig. 3. (A) The ECL signals of the prepared sensor with the variation of MUC1 concentrations. (B) The calirating curve of the proposed sensor for detecting MUC1.

Table 2
Comparison of different MUC1 detection methods.

Method	Detection range	Detection limit	signal amplification strategy	Detection time	Refs.
electrochemical	1 nM − 1 μM	0.827 nM (0.25 μg/mL)	without signal amplification strategy	120 min	Deng et al. (2017)
fluorescence	0.001 − 20 ng/mL	0.23 pg/mL	rolling circle amplification	330 min	Yang et al. (2018)
ECL	1 fg/mL − 1 ng/m	0.62 fg/mL	catalyzed hairpin assembly	120 min	Jiang et al. (2017)
ECL	1 fg/mL − 100 pg/mL	0.31 fg/mL	target-catalyzed hairpin hybridization	120 min	Chen et al. (2017a)
ECL	100 fg/mL − 100 ng/mL	33.3 fg/mL	the enzyme-assisted DNA recycling	90 min	Hu et al. (2018)
ECL	1 fg/mL − 10 ng/mL	0.48 fg/mL	without signal amplification strategy	50 min	this work

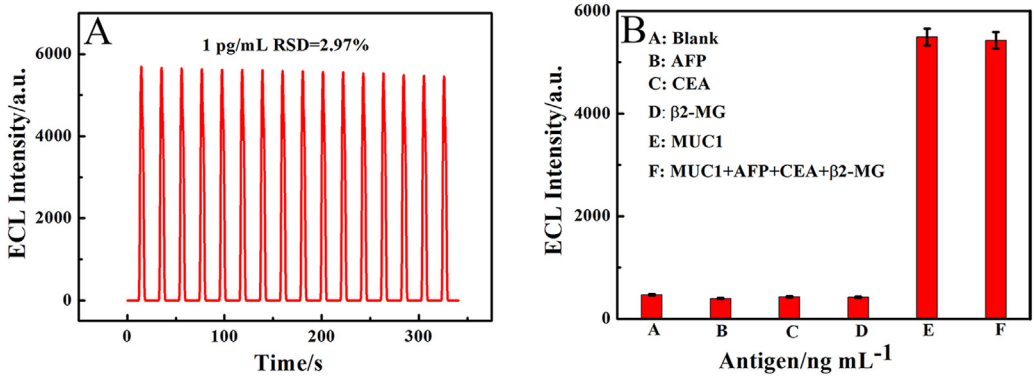

Fig. 4. (A) The stability of the prepared ECL sensor for 16 cycles with 1 pg/mL of MUC1. (B) Selectivity of the proposed immunosensor with different antigens.

particular, the detection limit of the proposed ECL sensor was 69 times lower than that of the ECL sensor based on PEI@Ru-PCN-777 with signal amplification strategy (Hu et al., 2018), highlighting the advantage of 2D MOLs over traditional 3D bulk MOFs as ECL tags. All these results indicated that the proposed ECL sensor may be an appropriate tool for simple, rapid and ultrasensitive detection of MUC1.

3.8. Stability and selectivity of the sensor

The stability of the prepared ECL sensor was investigated under a continuous scan with 1 pg/mL MUC1 for 16 cycles. As shown in Fig. 4A, the relative standard deviations (RSD) was 2.97%, demonstrating the ECL sensor possessed the high stability. Simultaneously, β2-microglobulin (β2-MG) (50 pg/mL), alpha-fetal protein (AFP) (50 pg/mL)

Table 3
The biosensor applied in real samples.

Sample number	Detection Times	Added (ng/mL)	Found (ng/mL)	Recovery (%)	RSD (%)
1	5	0.1	0.1046	104.6	7.4
2	5	0.5	0.4815	96.30	6.1
3	5	1	1.016	101.6	2.1
4	5	5	5.065	101.3	4.1

and carcinoembryonic antigen (CEA) (50 pg/mL) were used as interferences to evaluated the selectivity of the proposed sensor. As exhibited in Fig. 4B, the ECL intensity was almost no difference between the blank sample and these interferences. Moreover, compared with MUC1 (1 pg/mL), the ECL response of the ECL sensor incubated with the mixed samples was no significant changes. These results suggested that the prepared immunosensor possessed excellent selectivity for MUC1 detection.

3.9. Analysis of MUC1 in Human Serum

Recovery tests were performed in human serum for evaluating the feasibility of the ECL sensor. As listed in Table 3, the recovery was from 96.3% to 104.6% and RSD was from 2.1% to 7.4%, indicating that the immunosensor has favorable potential to detect MUC1 in real samples.

4. Conclusion

In summary, to increase the ECL efficiency and intensity, we have synthesized a highly stable Ru-Hf-MOL, which effectively shortens the transportation length of ion/electron, relieves the diffusional constraints of ion/electron, and possesses high loading number of Ru $(bpy)_2(mcpbpy)^{2+}$. As a result, the ECL efficiency and intensity of PEI@Ru-Hf-MOL are much higher than those of PEI@Ru-PCN-777. With the PEI@Ru-Hf-MOL as ECL indicators, the prepared immunosensor exhibits excellent selectivity, superior sensitivity and admirable stability for simple and rapid detection of MUC1. To our knowledge, this is the first example of an ECL sensor constructed by MOLs. Given that a lot of MOLs can be used to develop high-performance ECL materials, this work provided a new and feasible strategy to construct ultrasensitive ECL sensors, which greatly expanded the application of MOLs in bioanalysis.

Acknowledgments

This work was supported by the NSFC (21571149), NSF of Chongqing (cstc2016jcyjA0231, cstc2017jcyjAX0423), Innovation Support Program for Chongqing Overseas Returnees (cx2017007, cx2018026), and Selected Science Foundation for Overseas Chinese Returnees (2016).

Credit author statement

All authors have given approval to the final version of the manuscript.

Appendix A. Supporting information

Supplementary data associated with this article can be found in the online version at doi:10.1016/j.bios.2019.03.026.

References

Bossche, J.V., Al-Jamal, W.T., Tian, B., Nunes, A., Fabbro, C., Bianco, A., Prato, M., Kostarelos, K., 2010. Chem. Commun. 46, 7379–7381.
Cao, L.Y., Lin, Z.K., Shi, W.J., Wang, Z., Zhang, C.K., Hu, X.F., Wang, C., Lin, W.B., 2017. J. Am. Chem. Soc. 139, 7020–7029.
Cao, L.Y., Zhang, R., Zhang, W.Z., Du, Z.B., Liu, C.J., Ye, Z.Q., Song, B., Yuan, J.L., 2015. Biomaterials 68, 21–31.
Cao, L.Y., Lin, Z.K., Peng, F., Wang, W.W., Huang, R.Y., Wang, C., Yan, J.W., Liang, J., Zhang, Z.M., Zhang, T., Long, L.S., Sun, J.L., Lin, W.B., 2016. Angew. Chem. Int. Ed. 55, 4962–4966.
Chen, A.Y., Zhao, M., Zhuo, Y., Chai, Y.Q., Yuan, R., 2017a. Anal. Chem. 89, 9232–9238.
Chen, Q.S., Sun, J.L., Li, P., Hod, I., Moghadam, P.Z., Kean, Z.S., Snurr, R.Q., Hupp, J.T., Farha, O.K., Stoddart, J.F., 2016. J. Am. Chem. Soc. 138, 14242–14245.
Chen, Y., Zhou, S.W., Li, L.L., Zhu, J.J., 2017b. Nano Today 12, 98–115.
Cheng, A.K.H., Su, H.P., Wang, Y.A., Yu, H.Z., 2009. Anal. Chem. 81, 6130–6139.
Deng, C.Y., Pi, X.M., Qian, P., Chen, X.Q., Wu, W.M., Xiang, J., 2017. Anal. Chem. 89, 966–973.
Deria, P., Bury, W., Hod, I., Kung, C.W., Karagiaridi, O., Hupp, J.T., Farha, O.K., 2015. Inorg. Chem. 54, 2185–2192.
Deria, P., Bury, W., Hupp, J.T., Farha, O.K., 2014. Chem. Commun. 50, 1965–1968.
Ding, Y., Chen, Y.P., Zhang, X., Chen, L., Dong, Z., Jiang, H.L., Xu, H., Zhou, H.C., 2017. J. Am. Chem. Soc. 139, 9136–9139.
Dong, R., Pfeffermann, M., Liang, H., Zheng, Z., Zhu, X., Zhang, J., Feng, X., 2015. Angew. Chem. Int. Ed. 54, 12058–12063.
Easun, T.L., Moreau, F., Yan, Y., Yang, S., Schroder, M., 2017. Chem. Soc. Rev. 46, 239–274.
Ferreira, C.S.M., Papamichael, K., Guilbault, G., Schwarzacher, T., Gariepy, J., Missailidis, S., 2008. Anal. Bioanal. Chem. 390, 1039–1050.
Furukawa, H., Cordova, K.E., Keeffe, M.O., Yaghi, O.M., 2013. Science 341, 1230444.
Gui, G.F., Zhuo, Y., Chai, Y.Q., Xiang, Y., Yuan, R., 2014. Anal. Chem. 86, 5873–5880.
He, J.H., Zhang, G.J., Xiao, D.R., Chen, H.Y., Yan, S.W., Wang, X., Yang, J., Wang, E.B., 2012. CrystEngComm 14, 3609–3614.
Hu, G.B., Xiong, C.Y., Liang, W.B., Zeng, X.S., Xu, H.L., Yang, Y., Yao, L.Y., Yuan, R., Xiao, D.R., 2018. ACS Appl. Mater. Interfaces 10, 15913–15919.
Hu, J.M., Wang, T.Y., Kim, J., Shannon, C., Easle, C.J., 2012. J. Am. Chem. Soc. 134, 7066–7072.
Huang, Y., Zhao, M.T., Han, S.K., Lai, Z.C., Yang, J., Tan, C.L., Ma, Q.L., Lu, Q.P., Chen, J.Z., Zhang, X., Zhang, Z.C., Li, B., Chen, B., Zong, Y., Zhang, H., 2017. Adv. Mater. 29, 1700102.
Jiang, X.Y., Wang, H.J., Wang, H.J., Zhuo, Y., Yuan, R., Chai, Y.Q., 2017. Anal. Chem. 89, 4280–4286.
Kim, Y., Kim, J., 2014. Anal. Chem. 86, 1654–1660.
Kong, L.J., Zhu, J., Shuang, W., Bu, X.H., 2018. Adv. Energy Mater. 8, 1801515.
Kufe, D.W., 2009. Nat. Rev. Cancer 9, 874–885.
Lan, G.X., Li, Z., Veroneau, Samuel, S., Zhu, Y.Y., Xu, Z.W., Wang, C., Lin, W.B., 2018. J. Am. Chem. Soc. 140, 12369–12373.
Lan, G.X., Ni, K.Y., Xu, R.Y., Lu, K.D., Lin, Z.K., Chan, C., Lin, W.B., 2017. Angew. Chem. Int. Ed. 56, 12102–12106.
Li, F., Zhang, H., Lai, C., Li, X.F., Le, X.C., 2012. Angew. Chem. Int. Ed. 51, 9317–9320.
Li, L.L., Chen, Y., Zhu, J.J., 2017a. Anal. Chem. 89, 358–371.
Li, S.K., Liu, Z.T., Li, J.Y., Chen, A.Y., Chai, Y.Q., Yuan, R., Zhuo, Y., 2018. ACS Appl. Mater. Interfaces 10, 14483–14490.
Li, X., Li, Z.H., Lu, L., Huang, L.M., Xiang, L., Shen, J., Liu, S.Y., Xiao, D.R., 2017b. Chem. - Eur. J. 23, 10638–10643.
Lin, X.M., Luo, F.Q., Zheng, L.Y., Gao, G.M., Chi, Y.W., 2015. Anal. Chem. 87, 4864–4870.
Liu, S., Zhang, J.X., Tu, W.W., Bao, J.C., Dai, Z.H., 2014. Nanoscale 6, 2419–2425.
Liu, Z.Y., Qi, W.J., Xu, G.B., 2015. Chem. Soc. Rev. 44, 3117–3142.
Lu, Q.P., Zhao, M.T., Chen, J.Z., Chen, B., Tan, C.L., Zhang, X., Huang, Y., Yang, J., Cao, F.F., Yu, Y.F., Ping, J.F., Zhang, Z.C., Wu, X.J., Zhang, H., 2016. small 12, 4669–4674.
Nath, S., Mukherjee, P., 2014. Trends Mol. Med. 20, 332–342.
Parvin, N., Jin, Q., Wei, Y.Z., Yu, R.B., Zheng, B., Huang, L., Zhang, Y., Wang, L.H., Zhang, H., Gao, M.Y., Zhao, H.J., Hu, W.P., Li, Y.L., Wang, D., 2017. Adv. Mater. 29, 1606755.
Shi, W.J., Cao, L.Y., Zhang, H., Zhou, X., An, B., Lin, Z.K., Dai, R.H., Li, J.F., Wang, C., Lin, W.B., 2017. Angew. Chem. Int. Ed. 56, 9704–9709.
Si, H.B., Wang, L.J., Li, Q.L., Li, X.X., Li, L., Tang, B., 2018. Chem. Commun. 54, 8277–8280.
Song, F., Wang, C., Falkowski, J.M., Ma, L., Lin, W., 2010. J. Am. Chem. Soc. 132, 15390–15398.
Sun, X.P., Du, Y., Zhang, L.X., Dong, S.J., Wang, E.K., 2007. Anal. Chem. 79, 2588–2592.
Wang, D., Chai, Y.Q., Yuan, Y.L., Yuan, R., 2017a. Anal. Chem. 89, 8951–8956.
Wang, F., Lin, J., Zhao, T.B., Hu, D.D., Wu, T., Liu, Y., 2016a. J. Am. Chem. Soc. 138, 7718–7724.
Wang, H.J., He, Y., Chai, Y.Q., Yuan, R., 2014. Nanoscale 6, 10316–10322.
Wang, H.S., Liu, H.L., Wang, K., Ding, Y., Xu, J.J., Xia, X.H., Chen, H.Y., 2017b. Anal. Chem. 89, 11366–11371.
Wang, J.X., Zhuo, Y., Zhou, Y., Wang, H.J., Yuan, R., Chai, Y.Q., 2016b. ACS Appl. Mater. Interfaces 8, 12968–12975.
Wang, J.X., Zhuo, Y., Zhou, Y., Yuan, R., Chai, Y.Q., 2015. Biosens. Bioelectron. 71, 407–413.
Wang, S., Wang, Q.Y., Shao, P.P., Han, Y.Z., Gao, X., Ma, L., Yuan, S., Ma, X.J., Zhou, J.W., Feng, X., Wang, B., 2017c. J. Am. Chem. Soc. 139, 4258–4261.
Wang, Z.L., Jiang, X.Y., Yuan, R., Chai, Y.Q., 2018. Biosens. Bioelectron. 121, 250–256.
Wen, W., Hu, R., Bao, T., Zhang, X.H., Wang, S.F., 2015. Biosens. Bioelectron. 71, 13–17.
Wu, P., Hou, X.D., Xu, J.J., Chen, H.Y., 2014. Chem. Rev. 114, 11027–11059.
Xiao, D.R., Chen, H.Y., Chen, D.Z., He, J.H., Yan, S.W., Yang, J., Wang, X., Yuan, R., Wang, E.B., 2012. CrystEngComm 14, 2849–2858.
Xiong, C.Y., Liang, W.B., Zheng, Y.N., Zhuo, Y., Chai, Y.Q., Yuan, R., 2017. Anal. Chem. 89, 3222–3227.
Yang, L., Li, Y.Y., Zhang, Y., Fan, D.W., Pang, X.H., Wei, Q., Du, B., 2017. ACS Appl.

Mater. Interfaces 9, 35260–35267.
Yang, W.T., Shen, Y., Zhang, D.Y., Xu, W.J., 2018. Chem. Commun. 54, 10195–10198.
Zhang, H.T., Zhang, J.W., Huang, G., Du, Z.Y., Jiang, H.L., 2014. Chem. Commun. 50, 12069–12072.
Zhang, L., He, Y., Wang, H.J., Yuan, Y.L., Yuan, R., Chai, Y.Q., 2015. Biosens. Bioelectron. 74, 924–930.
Zhang, Y.L., Huang, Y., Jiang, J.H., Shen, G.L., Yu, R.Q., 2007. J. Am. Chem. Soc. 129, 15448–15449.
Zhao, M., Liao, N., Zhuo, Y., Chai, Y.Q., Wang, J.P., Yuan, R., 2015a. Anal. Chem. 87, 7602–7609.
Zhao, M., Zhuo, Y., Chai, Y.Q., Yuan, R., 2015b. Biomaterials 52, 476–483.
Zhao, M.T., Huang, Y., Peng, Y.W., Huang, Z.Q., Ma, Q.L., Zhang, H., 2018. Chem. Soc. Rev. 47, 6267–6295.
Zhao, M.T., Wang, Y.X., Ma, Q.L., Huang, Y., Zhang, X., Ping, J.F., Zhang, Z.C., Lu, Q.P., Yu, Y.F., Xu, H., Zhao, Y.L., Zhang, H., 2015c. Adv. Mater. 27, 7372–7378.
Zhao, Q.C., Zhou, Y.Y., Li, Y.Y., Gu, W., Zhang, Q., Liu, J., 2016. Anal. Chem. 88, 1892–1899.
Zhuo, Y., Liao, N., Chai, Y.Q., Gui, G.F., Zhao, M., Han, J., Xiang, Y., Yuan, R., 2014. Anal. Chem. 86, 1053–1060.